Self-Assembly of PLA-b-P3HT block copolymer

Letizia Ferbel, University of Pisa, Italy
Supervisors: Dr. Matthias Schwartzkopf, Msc. Marc Gensch
September 5, 2019

Abstract

Nowadays society demands for more and more energy and the only way to keep on providing the requested amount is to improve the efficiency of the renewable energy sources. In this work we will present a morphology development of a part of an active layer for organic solar cells with the goal of an effeciency improvement compared to bulk heterojunction organic solar cells. This work is based on the use of the biodegradable blockcopolymer PLA-b-P3HT, we will show how an ordered nanostructured surface with this block copolymer can be developed and its characteristics and nevertheless the processes that brought to its development.

Contents

1 Introduction

In the society we found ourselves today energy has become more and more demanded. In the past decade due to ecological issues and the reduction of non renewable energy sources, the energy provided by renewable-green sources, e.g. solar energy, wind power, hydropower etc., has importantly grown. An issue not to underestimate is the efficiency of the green sources, e.g. solar cells which convert solar energy in electricity via photovoltaics have an efficiency estimated around $23 - 25\%$, the Si based ones, and around 17% organic ones. At the moment results organic solar cells efficiency results very low but they have also the issue of fast degradation. A lot of efforts are nowadays made in order to solve this issues and to get a general improvent of the process. It is now known that to develop high performance organic and/or hybrid organic-inorganic solar energy devices, it is necessary to control the active layer morphology on the nanoscale.

What we would like to exploit in this work is an investigation of the morfology development of the material with as an ultimate future goal of efficiency improvement of organic solar cells (OSC) by designing an active layer of Poly(lactic acid)/poly(3-hexylthiophene) (PLA-b-P3HT) blockcopolymer.

The advantage of organic solar cells is the use of molecules such as polymers that are solution-processable at high throughput and cheap, resulting in low production costs to fabricate a large volume and also they have less adverse environmental impact. Combined with the flexibility of organic molecules, organic solar cells are potentially cost-effective for photovoltaic applications. Molecular engineering (e.g. changing the length and functional group of polymers) can change the band gap, allowing for electronic tunability. The optical absorption coefficient of organic molecules is high, so a large amount of light can be absorbed with a small amount of materials, usually on the order of hundreds of nanometers. Polymer solar cells also have the potential to exhibit transparency, suggesting applications in windows, walls, flexible electronics, etc.

The choice of PLA-b-P3HT has been made on the base of the work of Darling-Botiz [1]. We know that PLA-b-P3HT can undergo, under certain conditions, a microphase separation process and can lead to ordered morphologies on surfaces characterized by nanostructured domains of characteristic distance (tuned by the polymer block lengths). In particular the molecular weights of the two blocks encourage self-assembly into a lamellar structure. In this way, one can utilize rationally designed self-assembly to control the morphology at the nanoscale and thereby engineer enhanced effectiveness of internal processes. Moreover, since PLA block is biodegradable, once the phase separation of the two polymers is complete and the ordered nanoscale morphology is obtained, the PLA block can be removed and the space left can be used for example as a vessel for an acceptor material. [10] [12]

2 Experimental methods

The PLA-b-P3HT linear diblock copolymer was purchased as a custom synthesis from Polymer Source, Inc., and used without further purification. The polydispersity index

M_w/M_n was 1.45 as measured by the seller. The synthesised polymer has been first soluted with chloroform in order to obtain a liquid solution at different concentration specifically 5mg/mL, 10mg/mL, 15mg/mL, 20mg/mL, 25mg/mL. The solution has been subsequently spin coated on a cleaned pristine solid (100)-Si wafer. The spin coated sample have been further annealed in chloroform.
The analysis has been brought down firstly with AFM and subsequently using synchrotron radiation with GISAXS to complete the first rough analysis.
Samples showing a partially or fully developed lamellar structure have been subsequently sputtered in a sputtering chamber with 2nm film of silver. These samples have also been later analyzed using AFM and GISAXS.

2.1 Spin Coating

Spin coating is a fabrication method used to create thin films by depositing uniform coating of materials in solution on a flat surface.

Spin coating is a four step process, i.e. spin up, deposition, spin off and evaporation; first and second step in particular, can be used also in opposite order. In the following Figure (fig.1) is possible to graphically visualize the steps of the process

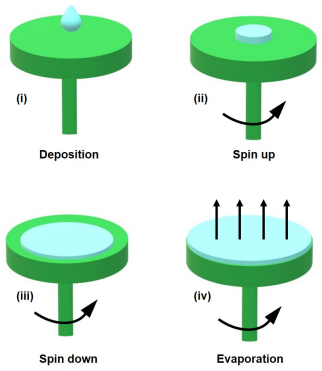

Figure 1: Steps of spin coating on a substrate

The first step is needed to set the parameters for the turntable such as ramp, rpm and spinning time; in the following step, i.e. deposition, we use an eppendorf pipet containing the solution one need to deposit and due to centrifugal force the solution will then be spread and distributed on the substrate. The spinning speed will determine the thickness of the layer (to note that this is not the only factor determining the thickness, for example the viscosity of the solution plays the major role). Subsequently there will follow spin off and evaporation steps: high volatile components are removed from the substrate because of either evaporation or drying meanwhile the low volatile components of the solution will remain on the surface. To note that during the spin coating process the solvent is partially or entirely removed by evaporation. [2]

2.2 Solvent Vapor Annealing (SVA)

One of the goal of this work is to process an ordered nanostructure but only solution deposition itself does not result in a highly ordered self-assembled nanostructure. Solution deposition suffers from the occurrence of secondary processes which are deterimental to attaining long-range molecular ordering in the deposited structures.

It has been seen that solvent vapour annealing (SVA) helps to increase the ordering in the self-assembly process. It is based on positioning the deposited samples in an environment saturated with solvent vapours, in our case Chloroform was used. The solvent vapor increase the polymer chain mobility and causes it to swell the thin polymer film. The resulting reorganization of the functional materials at the surfaces is due to a partial re-solubilization of the deposited layers, allowing the molecules to rearrange into structures characterized by a higher degree of order as compared to the starting samples [3].

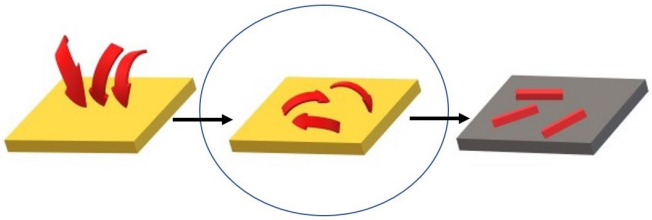

Figure 2: Solvent vapor annealing process

2.3 Sputtering

Coating methods include Physical Vapor Deposition (PVD) and one technique is called Sputtering. The sputtering method of thin film deposition involves introducing a controlled gas, usually chemically inert argon, into a vacuum chamber, and electrically energizing a cathode to establish a self sustaining plasma. The exposed surface of the cathode, called the target (in the case of the present work the target used is Silver), is a slab of the material to be coated onto the substrates. The substrate, i.e. the object to be coated is referred to as the substrate, and can be any of a wide variety of things such as: semiconductor wafers, solar cells, optical components. [4]

The gas atoms lose electrons inside the plasma to become positively charged ions, this happens because of the high voltage that is set between the anode and cathode which leads to a high impact ionization. The positive charged ions are then accelerated into the target and strike with sufficient kinetic energy to dislodge atoms or molecules of the target material. It can be thought of as a sort of atomic scale bead blasting. This sputtered material now constitutes a vapor stream, which traverses the chamber and hits the substrate, sticking to it as a coating or "thin film". [5] [11] Sputtering process is shown in Figure 3.

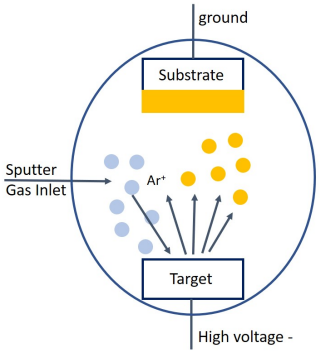

Figure 3: Sputtering process schematic

2.4 AFM

The Atomic Force Microscope (AFM) is one type of scanning probe microscopes, It is used to image surface structures (on a nm or even sub-nm scale scale) or to measure surface forces; the main advantages are that it takes a very small time to scan a sample, it needs very low sample preparation and more importantly it can reach a lateral resolution of 0.1 to 10 nm.

The standard AFM contains a microscopic tip (curvature radius of ∼10-50nm) attached to a cantilever spring. The underlying principle of AFM is the detection of the bending of this cantilever spring as a response to external forces. In the case of adhesive interaction between the tip and a surface, this forces are of the order 0.1-1 nN. To measure such small forces one must use not only very sensitive force-measuring springs but also very sensitive ways for measuring their bending. In order to detect this bending, which is as small as 0.01 nm, a laser beam is focused on the back of the cantilever. From there the laser beam is reflected towards a position-sensitive photodetector. Depending on the cantilever deflection the position of the reflected beam changes. The photodetector converts this change in an electrical signal.

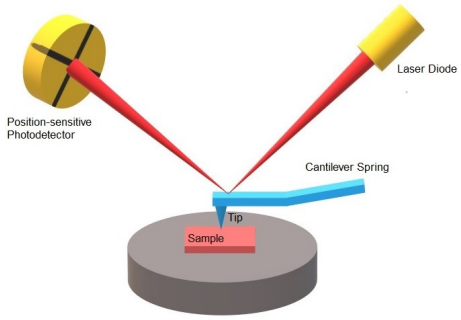

Figure 4: AFM schematics

A way to get information on the surface forces which are acting in a given system

and to illustrate the functioning of an AFM, is to use the Force Mode. This is done by moving the tip towards and away from the surface. Recording photodetector signal as a function of z-piezo elongation yields a curve which can be interpreted as a force-vs.-distance-curve.

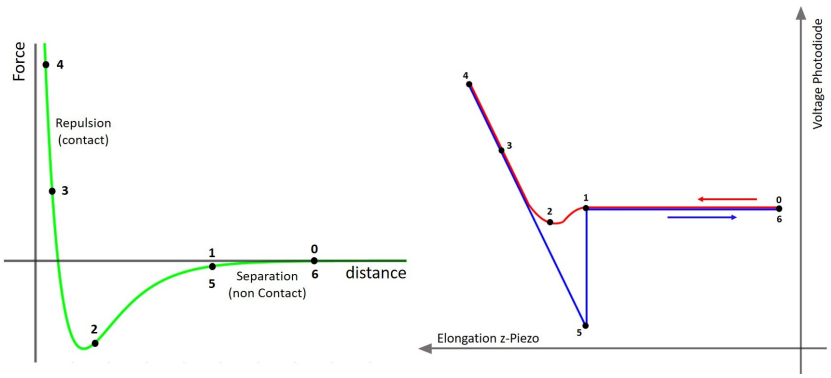

Figure 5: AFM Force Mode

Assuming that the tip-surface interaction can be described by a Lennard-Jones-Potential one can observe a cycle as follows: (0) the tip is far away from the surface, and surface forces do not act. As the tip approaches (1) to (2), it enters the range of attractive surface forces and is deflected downwards. (2) to (4): the tip is in contact with the surface and now exerts pressure while it is deflected upwards. At (4) the tip retraction started, but adhesion forces may keep the tip attached to the surface until the spring force exerted by the cantilever can overcome adhesion (5). Then the tip snaps back into its initial position and the cycle can start again (6). Force curves convey valuable information on the nature and strength of surface forces.

To acquire a surface image the AFM tip is brought down to the surface. A piezo element is used to scan the tip line by line across the sample. Since Contact mode may lead to structure damages, especially on soft surfaces (like the one we study in this work), for this kind of samples the so called Tapping Mode is used in general. In this mode the cantilever tip is stimulated to vibrations near the resonance frequency (∼300kHz). On approach to the surface, the vibration amplitude of the cantilever will decrease, since the interaction force with the surface shifts the resonance frequency. Instead of scanning the sample at constant deflection, the surface is scanned at constant reduction of the oscillation amplitude. As a result the tip is not in mechanical contact with the surface during the scan. The tapping mode is less destructive then the contact mode, because the exerted forces are in the pN range [6].

2.5 GISAXS

Classical nanoscale structural methods, such as atomic force microscopy (AFM) and transmission electron microscopy (TEM), provide highly precise local information about the nanostructured surface. However, with these methods, averaged (i.e. representative)

results can hardly be obtained from a sample. Grazing-incidence small-angle X-ray scattering (GISAXS) ideally complements these microscopic methods since it readily provides representative structural information for a large sample area in a very short time.

In the last years the number of GISAXS investigations increased owing to the ability to perform such experiments at many experimental stations at synchrotron radiation sources. Also, with the ongoing development of strong radiation lab-sources, GISAXS is now available in smaller setups in many laboratories. For what concerns soft matter samples, an energy of the order of 10 keV is recommended/needed.

The investigation of coatings, films and particles on surfaces leads always to a highly intense scattering pattern, even for films of nanoscale thickness, because the x-ray beam path length through the film plane is sufficiently long. Detectable length scales from a few to hundreds of nanometers are not limited by a beamstop which covers the information near $q_y = 0$ due to the possibility to perform so-called out-of-plane scans in GISAXS geometry. Bulk scattering from the substrate is reduced because of the limited penetration depth of the incoming beam at grazing incidence angles near the critical angle of the substrate (on which the material is deposited). GISAXS can be applied to determine internal morphologies of thin films as well as top surface morphologies of films, coatings and substrates.

In Figure 6 is illustrated the geometry of a GISAXS experiment.

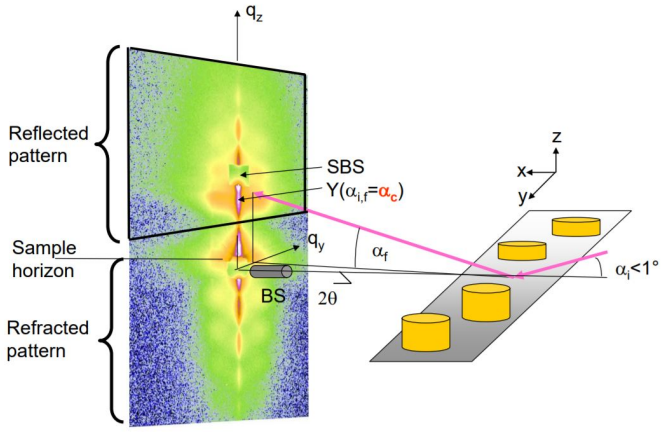

Figure 6: Geometry of a GISAXS experiment[8]

The sample is illuminated under grazing-incidence angle α_i, and the resulting reflected and scattered radiation is collected with a 2D detector at exit angles α_f and $2\theta_f$. The chosen coordinate system is such that the x–y-plane is the sample plane and the x-axis lies in the scattering plane, with the z-axis perpendicular to the sample plane. In

this coordinate system, the appearing scattering vector $q = k_f - k_i$ takes the form

$$\vec{q} = \frac{2\pi}{\lambda} \begin{pmatrix} \cos(\alpha_f)\cos(2\theta_f) - \cos(\alpha_i) \\ \cos(\alpha_f)\sin(2\theta_f) \\ \sin(\alpha_f) + \sin(\alpha_i) \end{pmatrix} \tag{1}$$

with the wavevector of the incoming beam k_i, the wavevector of the scattered beam k_f, $k = |k_i| = |k_f| = 2\pi/\lambda$, and the wavelength of the incident radiation λ.

In general, a 2D detector records the scattered intensity at angles of a few degrees for the observation of lateral sizes ranging from a few up to hundreds of nanometers. The sample detector distance is normally in a range of 1 to 4 meters for GISAXS, and up to 13 meters for grazing incidence ultra small angle scattering (GIUSAXS) experiments whereas the detectable lateral size increases to several micrometers. CCD-detectors as well as imaging plates are in use. The direct and the reflected specular beam are often suppressed by two small beamstops to prevent damage or saturation of the detector.

The scattering intensity I(q) for a lateral electron density fluctuation on the surface can be described as

$$I(\vec{q}) = \langle |F|^2 \rangle \, S(q_{||}) \tag{2}$$

where F is the form factor and $S(q)$ is the total interference function. The interference function describes the spatial arrangement of the objects on the surface and thus their lateral correlations. It is the Fourier transform of the island position autocorrelation function. In the simple Born approximation (BA), F is the Fourier transform of the shape function of the objects and is defined as

$$F(\vec{q}) = \int_V \exp(i\vec{q} \cdot \vec{r}) d^3r \tag{3}$$

If reflection-refraction effects at the surface of the substrate have to be accounted for, F has to be calculated within the distorted wave Born approximation (DWBA) and has a more complex expression. [7][9]

In order to analyze the GISAXS data files a software is needed. In this analysis DPDAK has been used for calibration and correction of raw data, one- or two-dimensional integration, as well as fitting and further analysis of the data, including the extraction of certain parameters. In particular from the line cuts in vertical and horizontal directions of the GISAXS pattern, i.e. Detector and Yoneda cut, one can obtain information about the film thickness, surface roughness and average nanostructural order of the sample. [**?**]

3 Results and discussion

Figure 7 shows the surface morfology of the samples at different diblock concentration just after spin coating
What needs to be remarked here is that the parameters of the spin coater as the quantity

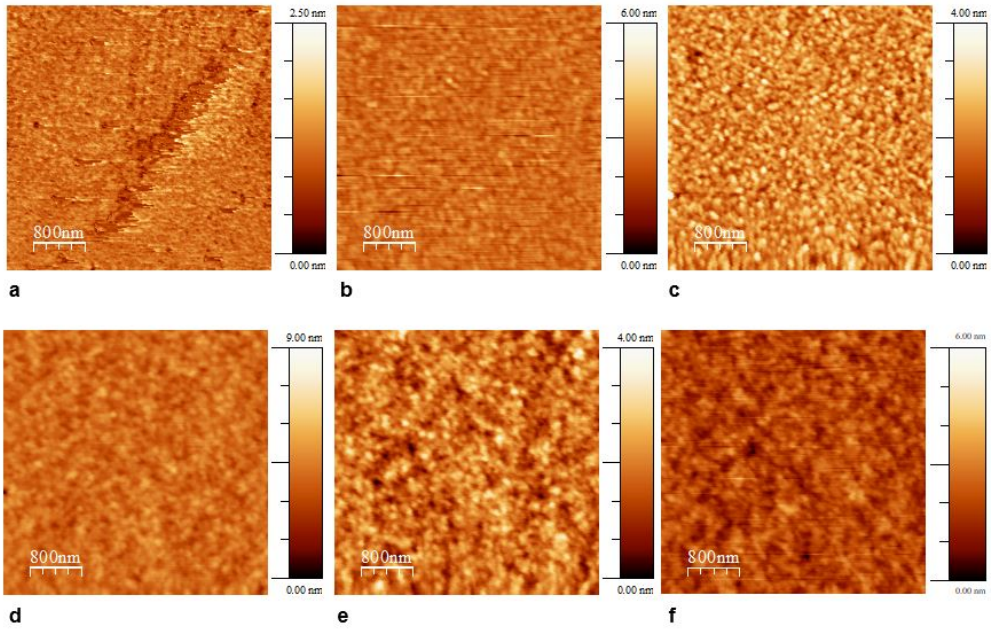

Figure 7: Reference Samples right after spin coating. $4\mu m \times 4\mu m$ AFM height image of a) pristine Si wafer, b) 5mg/mL, c) 10mg/mL, d) 15mg/mL, e) 20mg/mL, f) 25mg/mL

of the solution to spin coat have been carefully chosen in order to obtain an initial surface as smooth and as uniform as possible.

From the analysis of the samples roughness we found out that all the reference sample present an $RMS \sim 0.3 - 0.5$ which is of the same magnitude of the $RMS \sim 0.23$ of the substrate, i.e. the Si wafer, this results confirm our working hypothesis, i.e. having smooth surface also after spin coating and at higher diblock concentrations.

In two different beamtimes it was possible to take GISAXS images of some of the prepared samples with a beam energy of 6 GeV and a current $\sim$ 100 mA. Single shots of one reference sample look like Figure 8

Analyzing the Yoneda cut, i.e. a horizontal cut of the GISAXS spectrum (Fig.8) it is possible to extract information about the homogeneity and the distance between the materials on the surface of the film inspected.

Already looking at the AFM images in Figure 7 one can see the presence of darker and lighter spots that due to the fact that the P3HT before annealing present also a slightly hexagonal ordering and already from AFM images one can see that the samples do not show any or just a little ordering. In Figure 9 three 2D plots of the Yoneda cut are shown, in particular what is interesting is the difference among them. The side peak in the three plots is seen to move toward the $q_y = 0$ (here in the plot q_y =x-Axis) from the position and the broadening one can get two information: the average distance between the structures on the surface and their distribution. All the Yoneda plots show the presence of a side peak suggesting that the samples show already a sort of ordering

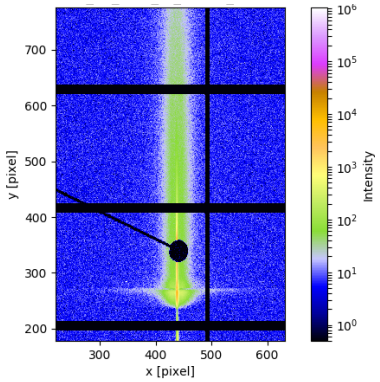

Figure 8: GISAXS Image Display

and so the formation of a nanostructure even though the side peaks are very broad. The moving maxima in q_y direction shows different size distributions for the concentrations, the more the side peak is close to the value $q_y = 0$ the larger is the average distance between the surface structures.

Instead from the 2D integration of the Detector cut, i.e. a vertical cut of the GISAXS spectrum (fig.8), it is possible to estimate the thickness of the deposited film.
The thickness of the film result from an analysis of the minima present in the plot shown in Figure 10, specifically if d is the distance between two minima, than the thickness of the film (t) is given by this simple formula $t = \frac{2\pi}{d}$.
The same analysis can be done using the AFM. What one can do is to scratch the surface of the sample in order to get a cut through the film exposing than the Si surface.
As shown in Figure 11 once a scan of the scratch has been made it is necessary to adjust the image in order to get a flat Silicon surface an just by the difference in height between the side with the film (Figure 11 on the right side) and the Si side (Figure 11 on the left side) it is possible to estimate the film thickness.
The GISAXS analysis and the AFM results are in good agreement among them and they showed an increasing thickness of the film with respect of the concentration of the diblock, as we also expected. In particular we found the following film thickness distribution

Concentration (mg/mL)	5	10	15	20	25
t (nm)	17	39	54	81	98

As already mentioned above, the PLA-b-P3HT block copolymer after annealing, here performed in chloroform, undergoes different morphology changes (ref. [1]). In this work, we wanted to study these reordering transitions to better understand the factors that govern the order seen in the final state, i.e. the lamellar morphology. In this initial part of the project we focussed mainly on the study of morphology changes of the block copolymer in concentrations 5mg/mL and 20 mg/mL there could be two reasons for this: first of all, there is a big difference in viscosity of the polymer and in the thickness of the deposited film and second because we saw that there is a relation of

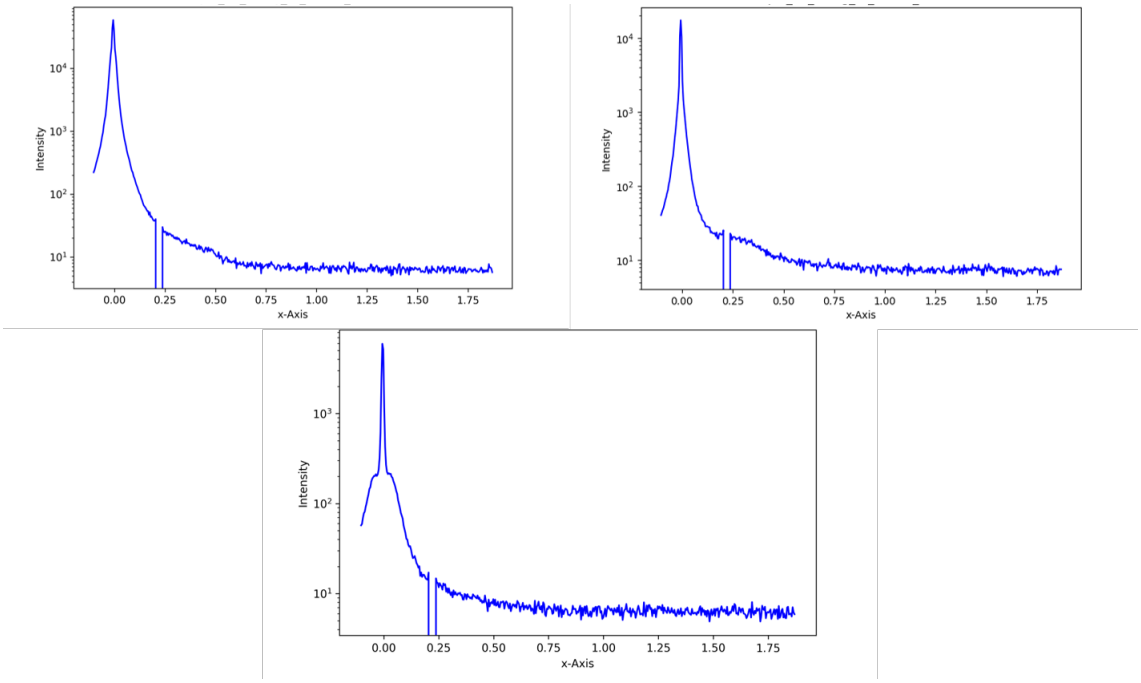

Figure 9: Yoneda Cut of 20mg/mL, 15mg/mL and 5mg/mL reference samples

inverse proportionality of some kind between the annealing time and the concentration. As we can see in Figure 12, with solvent vapor annealing in chloroform the samples undergo a morphology change, both the concentrations 5mg/mL and 20 mg/mL showed good results even though we were not able to find at this point the right parameters for a reproducible lamellar structure

The main difference that we can spot form these AFM images is the dimension of the just formed structure, in the 20mg/mL samples compared to the samples with 5 mg/mL the lamellae showed a smaller lateral extension and the structures are longer with a larger peak to valley distance (Figure not shown).

The main problem we encountered is related to the chemical nature of this block copolymer. We saw that it is very reactive to humidity in particular it is an hydriphilic polymer and that prevented us to reproduce the same sample using the same parameter and getting the same results also with humidity changes within 5%.

Lastly we chose a sample that showed good characteristics, i.e. a step forward to lamellar formation, and sputtered on it 2 nm of Silver.
From both the height and the phase images (Figure 13) we can see that the deposited silver reproduced the pattern of the film underneath.

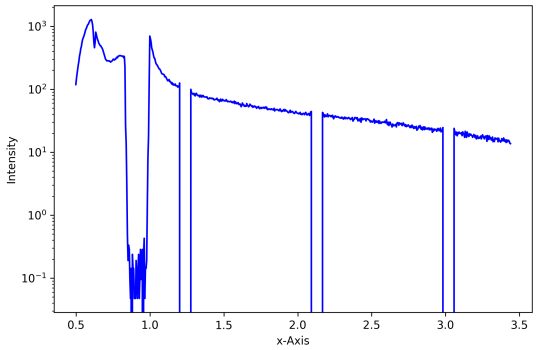

Figure 10: Detector CUT (the discontinuity of the curve are due to the mask and the beamstop covering the detector)

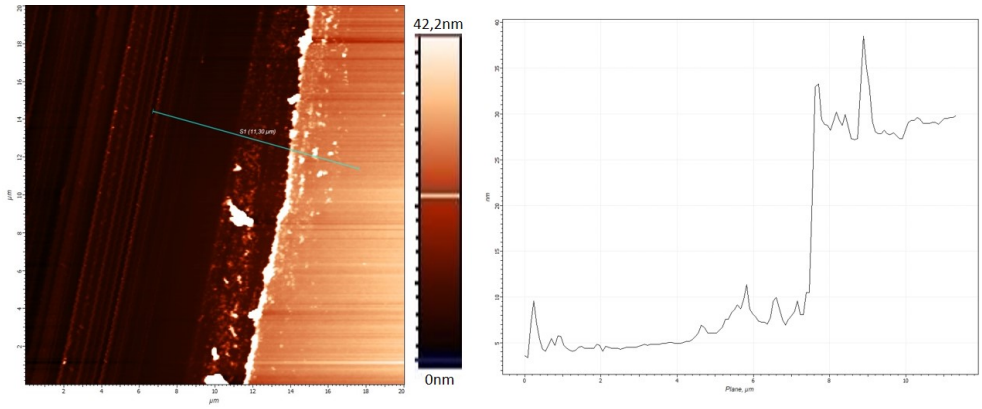

Figure 11: AFM scan of height profile of the cut and plot of the line cut through the cut

4 Conclusion

We managed to get smooth and homogeneous surfaces at all concentration before annealing.
Despite all the problems present at this point of the investigation we managed anyway to see what we expected after annealing meaning that there is definitely a morphology change and there is a possibility to get to a lamellar structure.
The silver can deposit on the prepattern surface and follow the morfology confirming the possibility using this block copolymer in different fields.

In the future will be necessary to prepare the samples in a humidity controlled environment and to analyze more samples using GISAXS or other instruments than AFM.
We can say that with this work we putted the basis for a forward investigation where the system can be better study since with this analysis it already showed promising results.

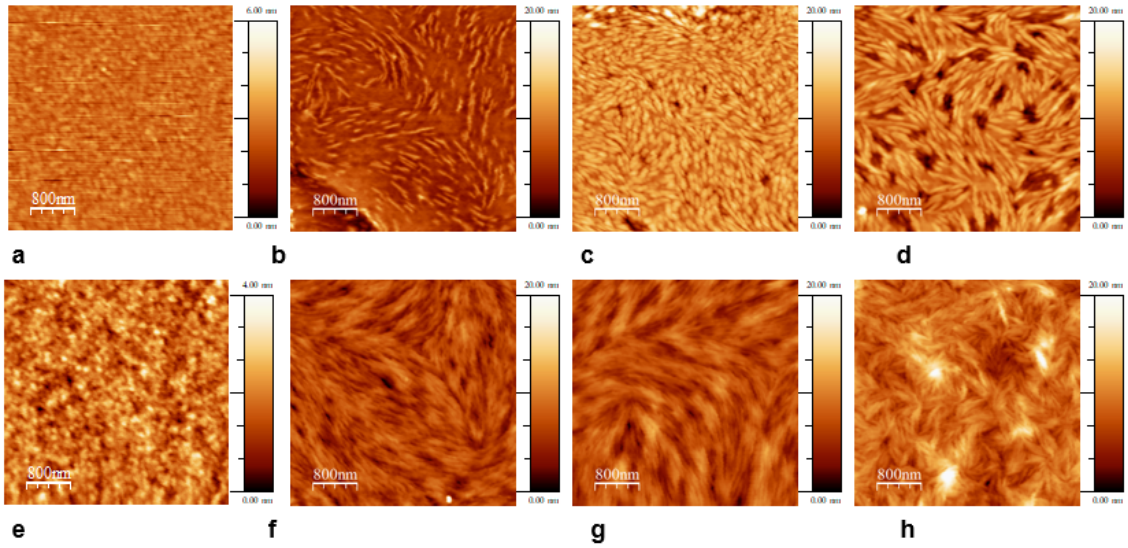

Figure 12: Lamellar structure evolution for increasing annealing time. 5mg/mL a), b), c), d) and 20mg/mL e), f), g), h)

Acknowledgment

I need first to thank DESY that have given me the opportunity to spend two months in their facility between lectures and laboratory experiences. My supervisor that gave me this interesting project. And of course I need to thank all the P03 group (Pallavi, Andrei, Matthias, Stefan and Andrea) for supporting and standing me in this long but short time. *Ad maiora!*

References

[1] Ioan Botiz and Seth B. Darling. *Self-Assembly of Poly(3-hexylthiophene)-block-polylactide Block Copolymer and Subsequent Incorporation of Electron Acceptor Material.* Macromolecules 2009, 42, 8211–8217.

[2] Bekir Sami Yilbas and Abdullah Al-Sharafi and Haider Ali. *Chapter 3 - Surfaces for Self-Cleaning.* Elsevier, Self-Cleaning of Surfaces and Water Droplet Mobility: 45 - 98, 2019.

[3] V. Palermo, P.Samori et al.. *Solvent vapour annealing of organic thin films: controlling the self-assembly of functional systems across multiple length scales.* J. Mater. Chem., 2010, 20, 2493–2498.

[4] Norm Hardy, Process Engineer - Semicore Equipment, Inc. `http://www.semicore.com/news/70-thin-film-deposition-sputtering`

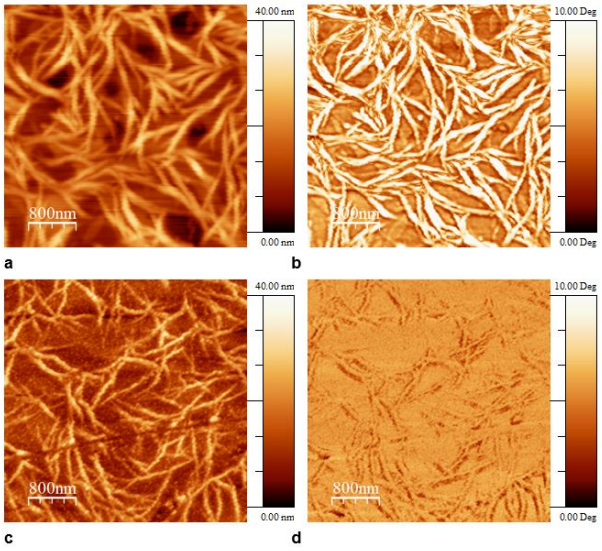

Figure 13: $4\mu m \times 4\mu m$ AFM image of a 5mg/mL sample height and phase image before sputtering deposition a), b), and after Ag deposition c) , d)

[5] Thin film consulting advancing magnetron sputtering technology.
`http://www.thfc.de/fundamentals-of-sputtering`

[6] C. Helm, Institute of Physics, University of Greifswald,
`https://physik.uni-greifswald.de/en/research-groups/`

[7] A. Meyer, Institute of Physical Chemistry, University of Hamburg,
`http://www.gisaxs.de`

[8] Methoden moderner Roentgenphysik II - Vorlesung im Haupt/Masterstudiengang Physik, Universität Hamburg, SS 2010 S.V. Roth
`http://photon-science.desy.de/sites/site_photonscience/content/e62/e189219/e189559/e189721/e189728/e189730/infoboxContent189738/roth_lecture_3_eng.pdf`

[9] Pflüger, Mika et al. *Grazing-incidence small-angle X-ray scattering (GISAXS) on small periodic targets using large beams.*. IUCrJ vol. 4,Pt 4 431-438. 24 May. 2017.

[10] Roberto Nisticò. *Block copolymers for designing nanostructured porous coatings.* Beilstein J. Nanotechnol. 2018, 9, 2332–2344.

[11] Schwartzkopf Matthias, Stephan V. Roth et all. *From atoms to layers: in situ gold cluster growth kinetics during sputter deposition.* Nanoscale 2013, issue 11, volume 5, 5053-5062.

[12] Marc Gensch, Schwartzkopf Matthias, Stephan V. Roth et all. *Correlating Nanostructure, Optical and Electronic Properties of Nanogranular Silver Lay-*

ers during Polymer-Template-Assisted Sputter Deposition. ACS Appl. Mater. Interfaces2019113229416-29426.

[13] Schwartzkopf Matthias, Stephan V. Roth. *Investigating Polymer–Metal Interfaces by Grazing Incidence Small-Angle X-Ray Scattering from Gradients to Real-Time Studies.* Nanomaterials (Basel). 2016 Dec; 6(12): 239.

[14] G. Benecke, W. Wagermaier, C. Li, M. Schwartzkopf, G. Flucke, R. Hoerth, I. Zizak, M. Burghammer, E. Metwalli, P. Müller-Buschbaum, M. Trebbin, S. Förster, O. Paris, S. V. Roth and P. Fratzl. *A customizable software for fast reduction and analysis of large X-ray scattering data sets: applications of the new DPDAK package to small-angle X-ray scattering and grazing-incidence small-angle X-ray scattering.* J. Appl. Cryst. (2014). 47, 1797-1803.